-Supporting Information-

Annealing 1,2,4-Triazine to Iridium(III) Complexes Induces Luminogenic Behaviour in Bioorthogonal Reactions with Stain Alkynes.

Lydia Cooke,[a] Katie Gristwood,[b] Kate Adamson,[a] Mark Sims,[a] Michael Deary,[a] Dawn Bruce,[a] Antony N. Antoniou,[a] Hannah R. Walden,[a] James Knight,[b] Timothé Antoine-Brunet,[c] Marie Joly,[c] David Goyard,[c] Pierre-Henri Lanoë,[c] Nathalie Berthet,[c] and Valery N. Kozhevnikov*[a]

[a] Department of Applied Sciences, Northumbria University, Ellison Building, Newcastle upon Tyne, NE1 8ST, U.K.

[b] School of Natural and Environmental Sciences, Newcastle University, Bedson Building, Newcastle upon Tyne NE1 7RU, U.K.

[c] Université Grenoble Alpes, CNRS, DCM UMR 5250, 38000 Grenoble, France.

Contents

Synthesis.

General

All solvents and reagents were purchased from commercial suppliers and used without further purification. NMR spectra were recorded on a JEOL ECS400FT Delta spectrometer (399.78 MHz for ^{1}H NMR). Chemical shifts are reported in parts per million (ppm) relative to a tetramethylsilane internal standard or to a residual solvent peak. All UV-Vis spectra were recorded on a Varian Cary 50 Bio UV-Visible Spectrophotmeter. HRMS analysis was performed on LTQ Orbitrap XL Thermo Scientific. Ac_4Man*N*BCN[1] and BCN-C10[2] were prepared as previously described.

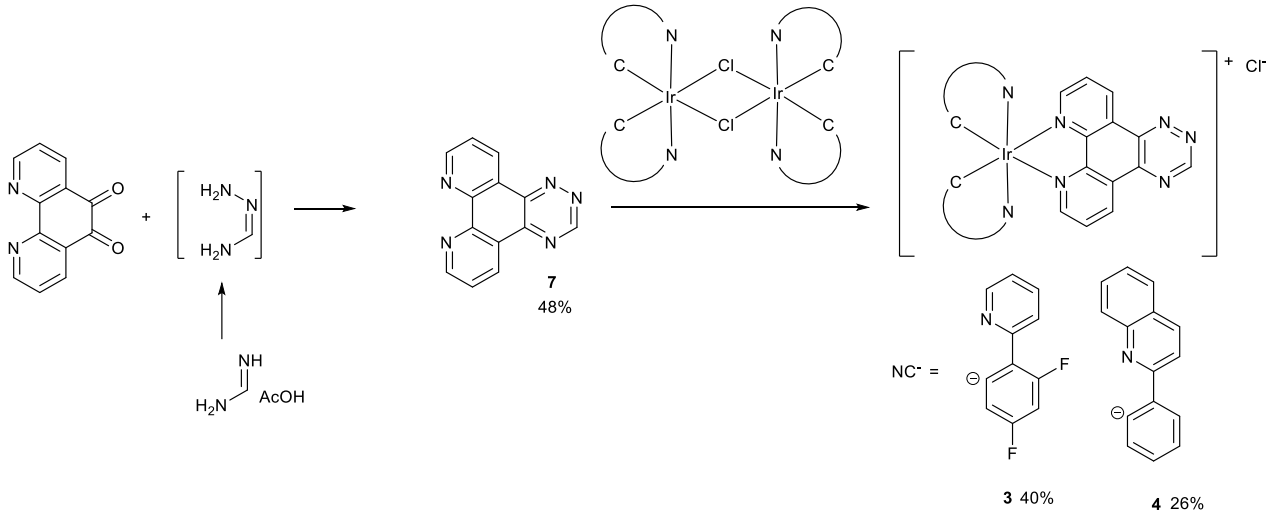

Scheme S1. Synthesis of the 1,2,4-triazine-containing ligand and its iridium complexes.

Synthesis of ligand 7 [3, 4]

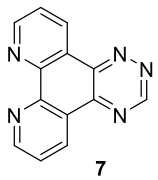

7

Hydrazine hydrate (143 mg, 2.86 mmol) was added to a solution of formamidinium acetate (346 mg, 3.33 mmol, 1.4 eq) in 15 mL of methanol. The mixture was stirred for 1 minute and then added to a solution of the 1,10-Phenanthroline-5,6-dione **1** (500 mg, 2.38 mmol, 1 eq.) in DMF (6 mL). The reaction mixture was stirred at room temperature for 16 h. The solvent was evaporated, the residue was treated with water and filtered. The solid on filter was washed with water (10 mL) and ethanol (10 mL) to give the desired product. Yield 267 mg (48%). ^{1}H NMR (400 MHz, $CDCl_3$) δ: 10.11 (s, 1H), 9.78 (d, J = 8.4 Hz, 1H), 9.55 (d, J = 8.4 Hz, 1H), 9.37-9.41 (m, 2H), 7.85-7.92 (m, 2H); ^{13}C NMR (100.6 M, $CDCl_3$) δ: 155.9, 154.9, 153.8, 149.7, 147.4, 146.2, 142.6, 134.3, 132.8, 125.3, 125.0, 124.9, 124.7.

Synthesis of complex 3

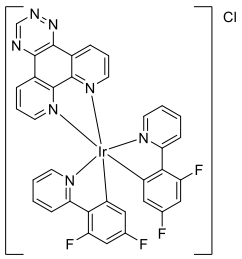

A mixture of the ligand **7** (120 mg, 0.515 mmol) was dissolved in a mixture of chloroform (10 mL) and methanol (10 mL). Dichloro-bridged complex $[Ir(dfppy)_2]_2Cl_2$ (228 mg, 0.36 mmol per Ir, 1 eq) was added. On addition of $[Ir(dfppy)_2]Cl_2$ a clear yellow solution turned to a dark red/brown colour. The reaction mixture was heated under reflux for 3 hours. All volatiles were then removed by rotary evaporation. The residue was treated with 30 mL of diethyl ether and the solid was filtered off. The product was purified by column chromatograph using silica gel and a mixture of DCM and methanol (20:1 vv). Yield 168 mg (40%).

^{1}H NMR (400 MHz, DMSO-D_6) δ: 10.48 (s, 1H), 9.91 (d, J = 8.4, 1H), 9.71 (d, J = 8.4, 1H), 8.46 (d, J = 5.0, 1H), 8.43 (d, J = 5.0, 1H), 8.19-8.28 (m, 4H), 7.98 (br.t, J = 7.8, 2H), 7.61 (d, J = 6.0, 2H), 6.97-7.10 (m, 4H), 5.66 (dd, J = 8.2, 2.0, 2H).

^{19}F NMR (100 MHz, DMSO-D_6) δ: -106.3, -108.5.

HRMS (ESI) calculated for $[M\text{-}Cl]^+$ $C_{35}H_{19}N_7F_4Ir$ 806.12635, found 806.12626.

Synthesis of complex **4**

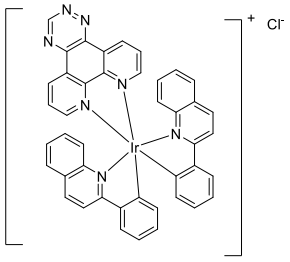

The ligand **7** (257 mg, 1.1 mmol, 1.1 eq) was dissolved in chloroform (25 mL). Methanol (25 mL) was added, followed by di-chlorobridged iridium complex (636 mg, 1 mmol for Ir). The mixture was stirred and heated under reflux for 3 hours. The solvent was evaporated. The residue was dissolved in methanol (15 mL) and filtered. The filtrate was evaporated to dryness. The residue was treated with diethyl ether. The solid formed was filtered off to give a crude product (410 mg). The product was then purified by silica column chromatography using DCM/MeOH, 10/1 as an eluent. The fractions containing product were combined and evaporated to a volume of approximately 3 mL and diethyl ether (20 mL) was added. The formed yellow-orange solid was filtered off, washed with diethyl ether to give after drying the desired product. Yield 230 mg (26%).

^{1}H NMR (400 MHz, DMSO-D_6) δ: 10.32 (s, 1H), 9.79 (d, *J* = 8.0, 1H), 9.59 (d, *J* = 8.0, 1H), 8.70 (d, *J* = 4.9, 1H), 8.68 (d, *J* = 4.9, 1H), 8.64 (dd, *J* = 8.6, 2.5, 2H), 8.54 (dd, *J* = 8.6, 2.5, 2H), 8.38 (d, *J* = 8.0, 2H), 8.29 (m, 2H), 7.84 (d, *J* = 8.0, 2H), 7.28 (t, *J* = 8.0, 2H), 7.24 (t, *J* = 8.0, 2H), 7.14 (br.t, *J* = 9.2, 2H), 6.90 (m, 4H), 6.50 (d, *J* = 7.8, 2H).

^{13}C NMR (100.6 M, DMSO-D_6, Me_4Si) δ: 170.2, 157.1, 152.1, 151.1, 150.3, 150.0, 148.0, 147.4, 146.4, 145.3, 142.3, 141.0, 136.6, 135.1, 134.6, 131.6, 131.2, 129.8, 128.4, 127.9, 127.3, 124.2, 123.6, 118.9.

HRMS (ESI) calculated for $[M\text{-}Cl]^+$ $C_{43}H_{27}N_7Ir$ 834.19542, found 834.19573.

Synthesis of complex **8**

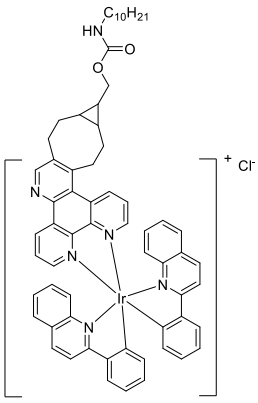

A mixture of **BCN-C10** (80 mg, 0.24 mmol) and complex **4** (87 mg, 0.1 mmol) in methanol (7 mL) was stirred at room temperature for 2 hours. TLC (DCM/methanol, 5/1 v/v) showed complete conversion. The mixture was evaporated to dryness. The mixture was triturated with petrol ether (10 mL) and the petrol ether was decanted. The residue was then triturated with diethyl ether (10 mL). Ultrasonic bath allowed to detach the product from the sides of the flask. The solid was filtered off to give a crude product (95 mg). The product was purified by column chromatography using small (diameter 1.5 cm) column, 9 g of silica gel and DCM/methanol 5/1 v/v mixture as an eluent. Yield 78 mg (66%). ^{1}H NMR (400 MHz, Methanol-D_4) is not well-resolved due to formation of mixture of stereoisomers. The copy of the NMR is given in figure S7. HRMS (ESI) calculated for $[M\text{-}Cl]^+$ $C_{64}H_{62}O_2N_6Ir$ 1139.45634, found 1139.45635

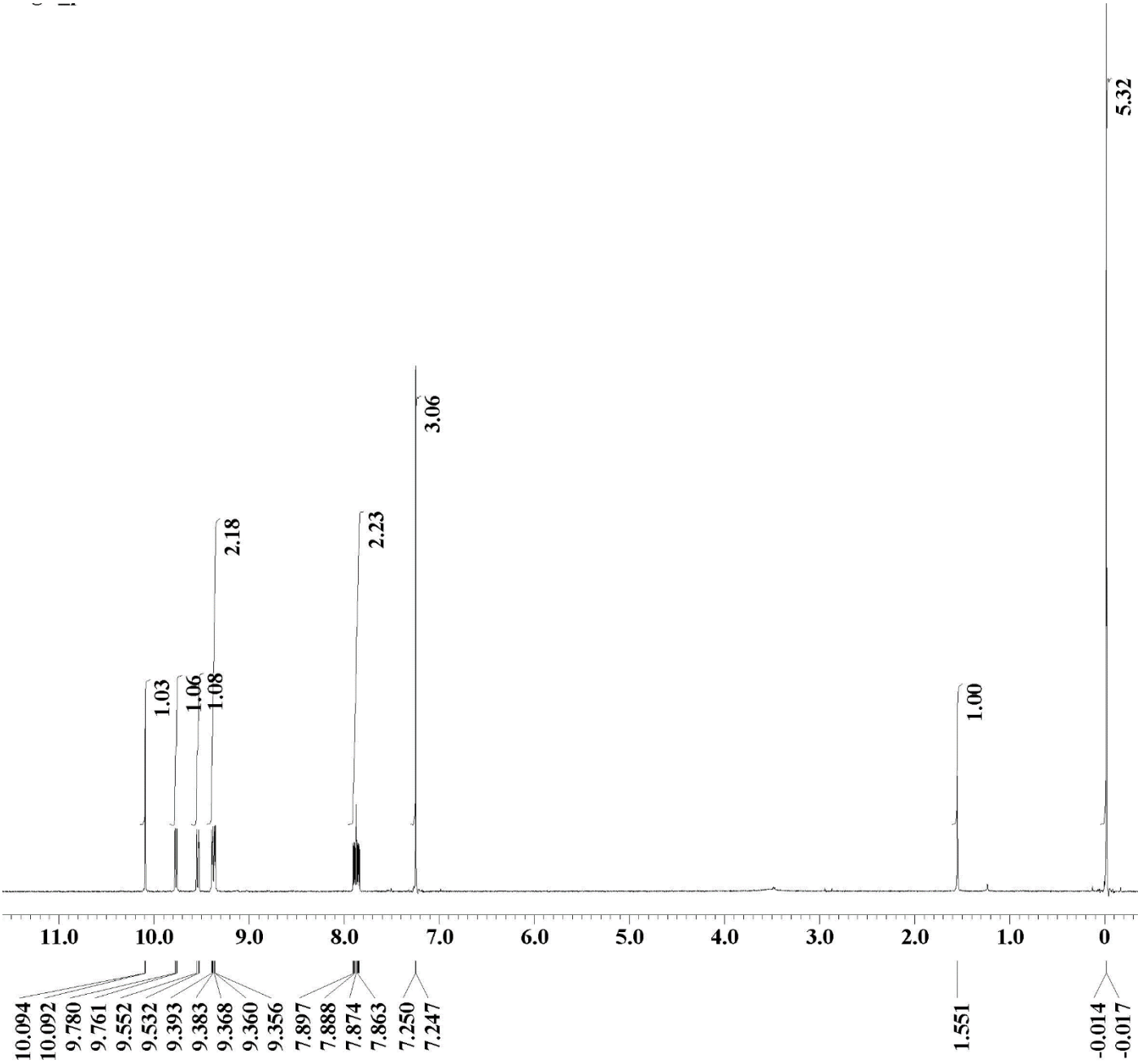

Figure S1. ^{1}H NMR of ligand **7** in $CDCl_3$

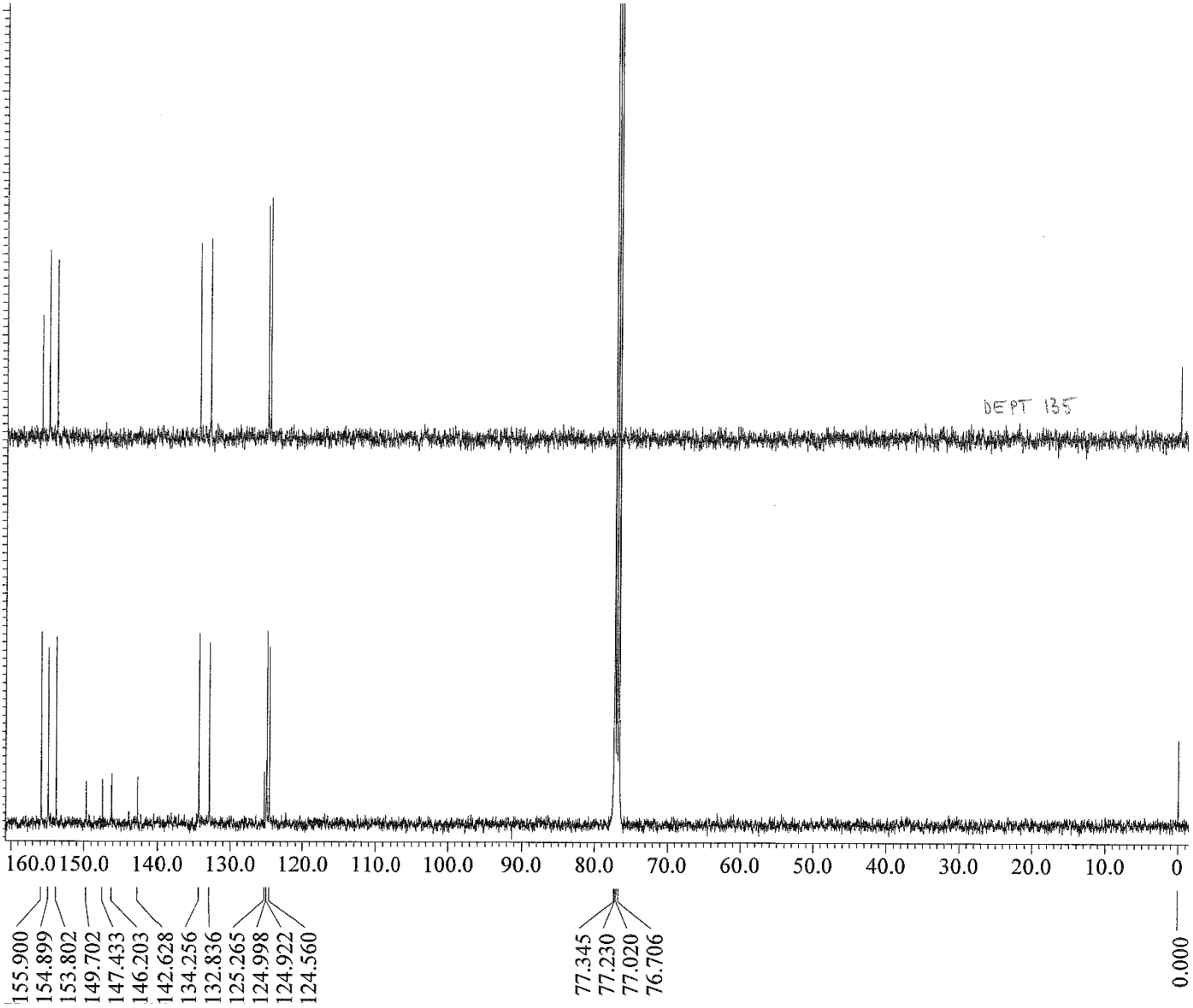

Figure S2. ^{13}C NMR of ligand **7** in $CDCl_3$

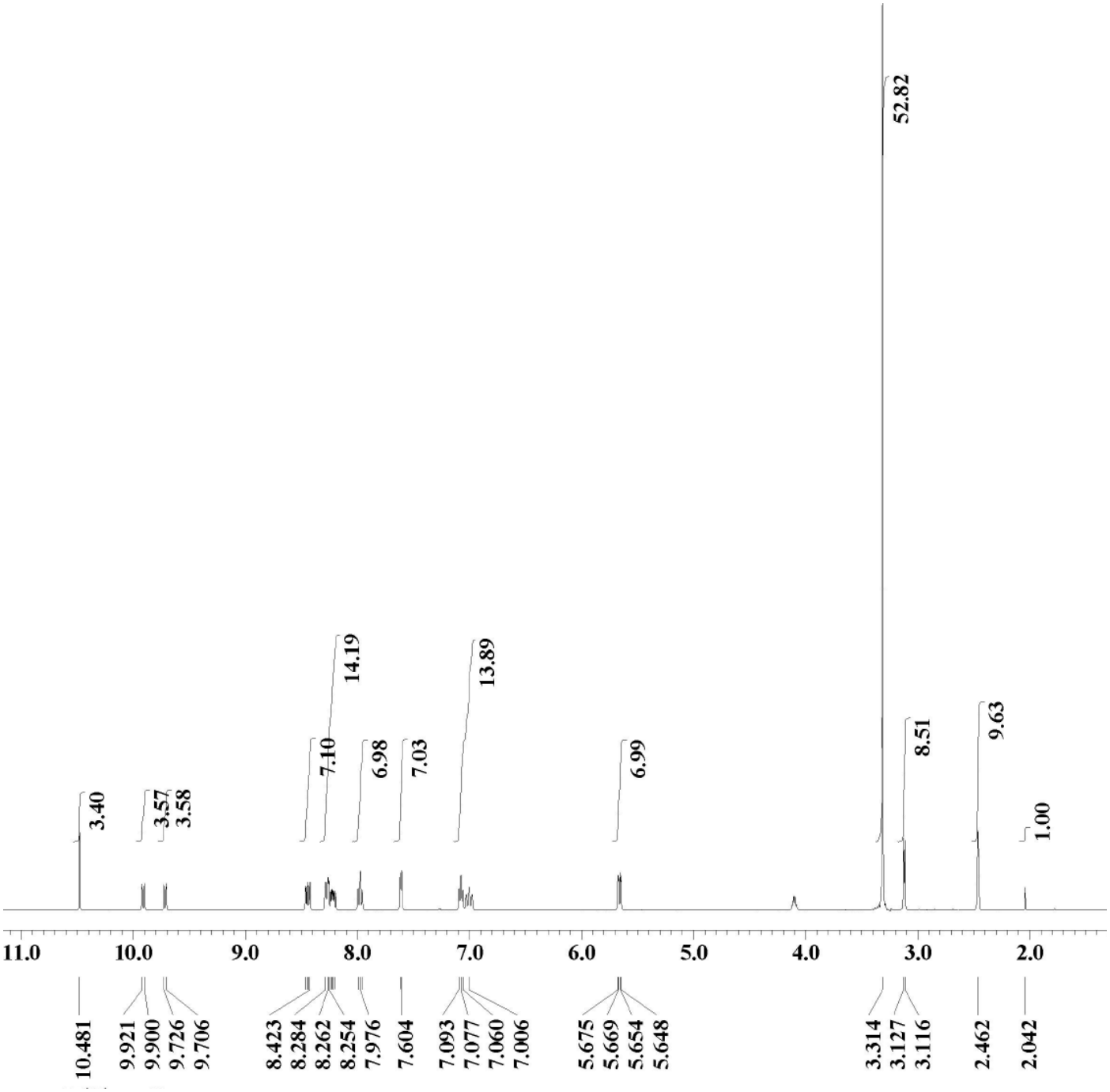

Figure S3. ^{1}H NMR of complex **3** in DMSO-D_6

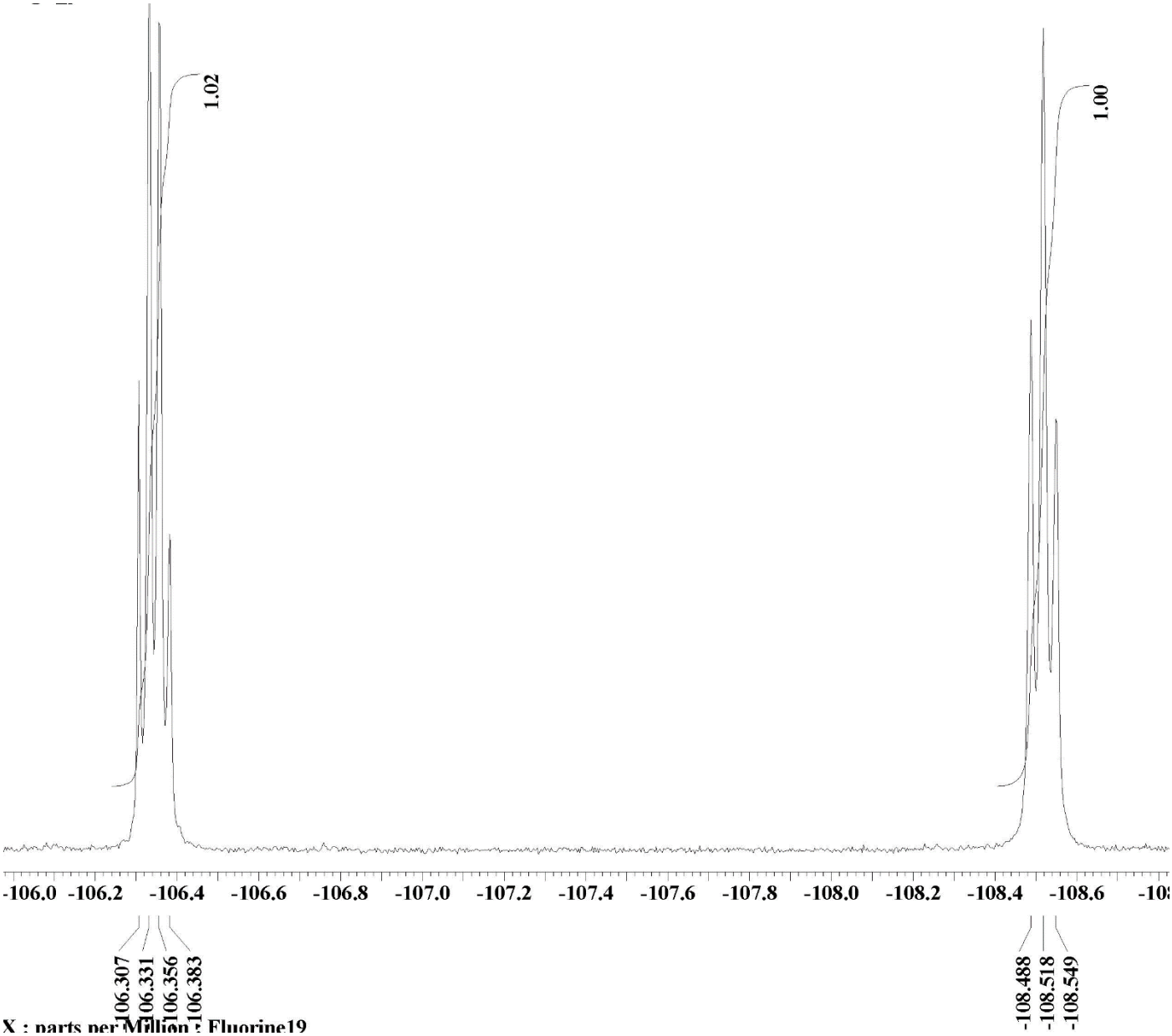

Figure S4. ^{19}F NMR of complex **3** in DMSO-D_6

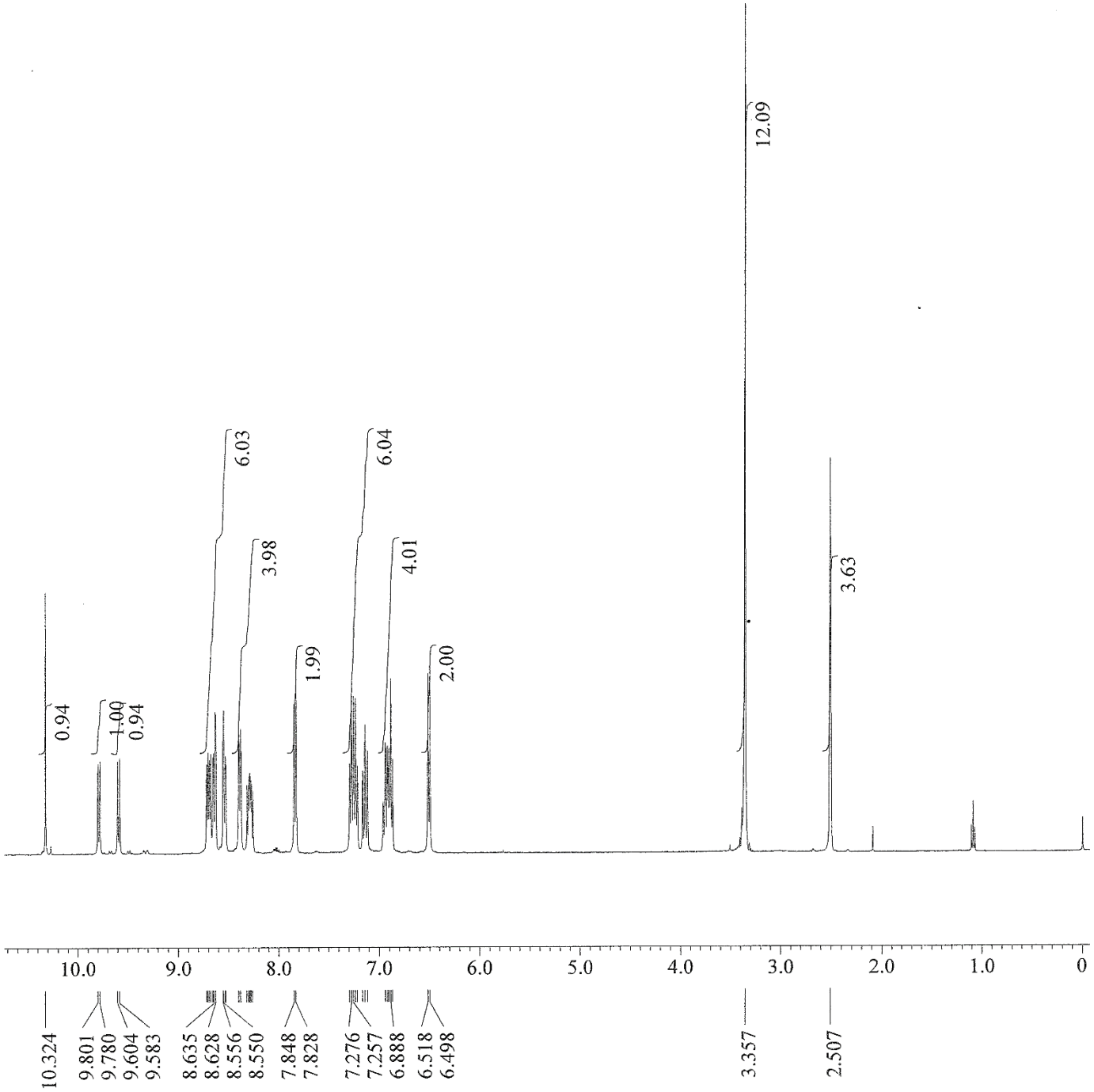

Figure S5. ^{1}H NMR of complex **4** in DMSO-D_6

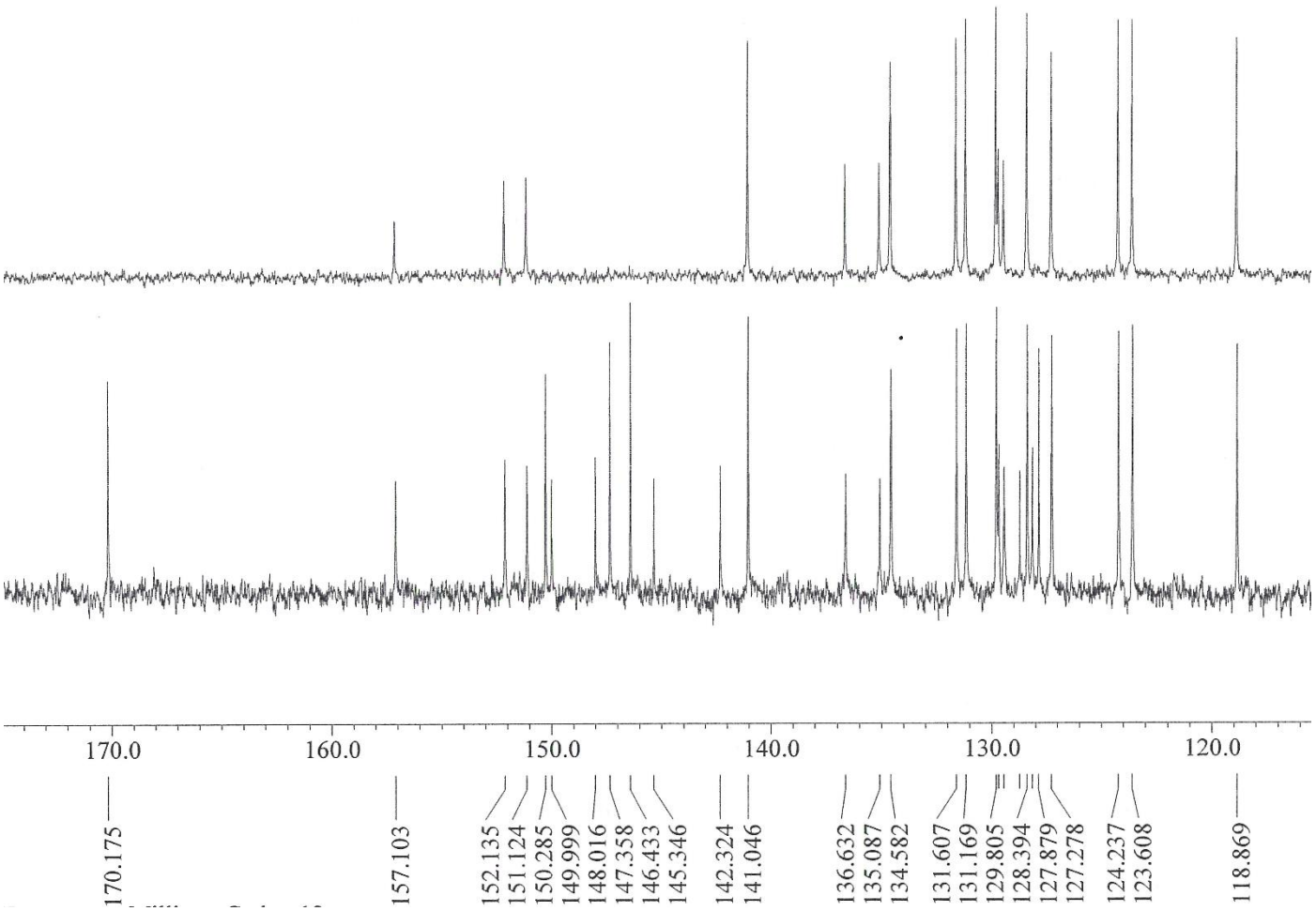

Figure S6. Aromatic region of ^{13}C NMR spectrum of complex **4** in DMSO-D_6 (the top spectrum is ^{13}C DEPT135)

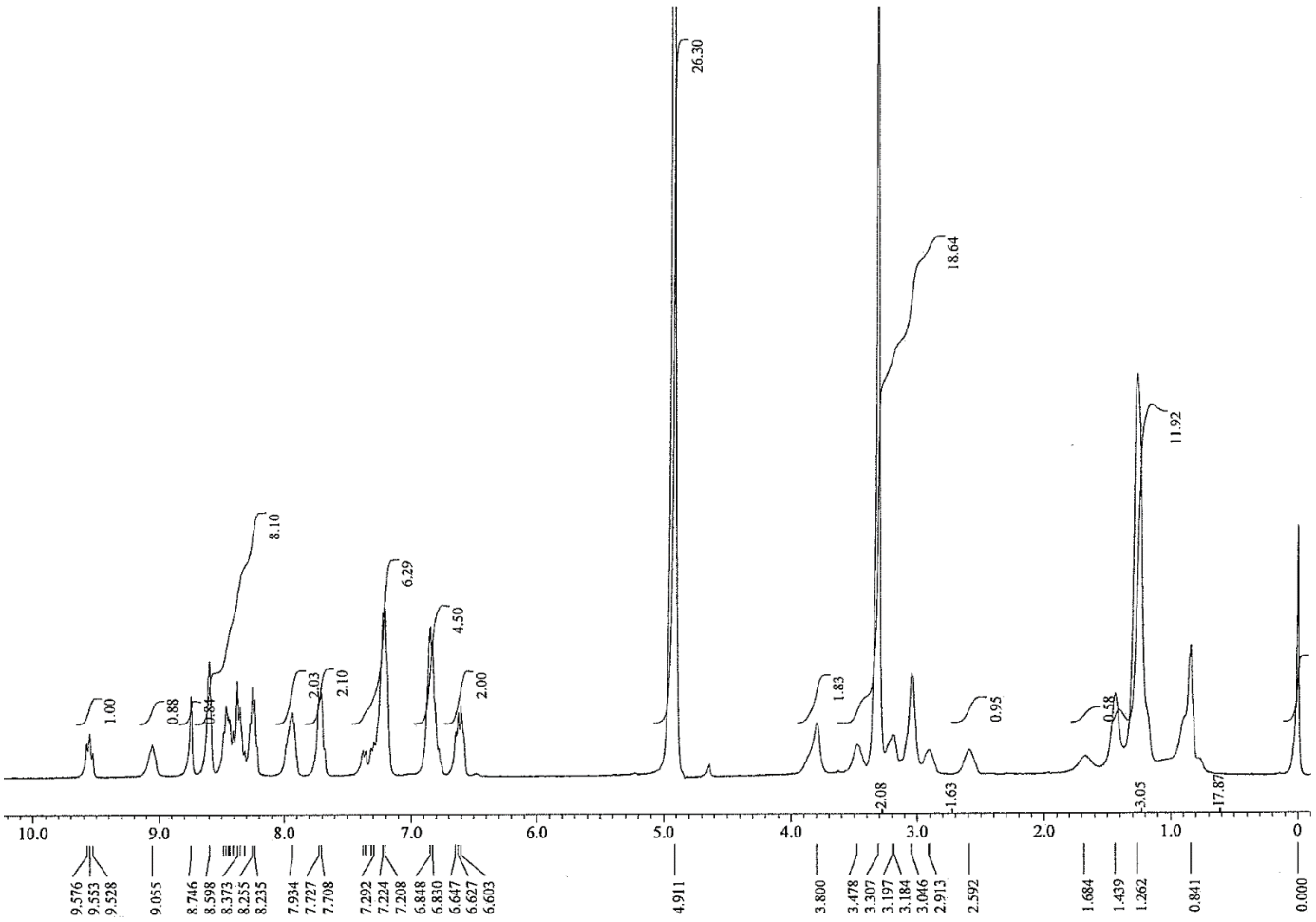

Figure S7. ^{1}H NMR of complex **8** in Methanol-D_4

Determination of second order rate constant

The reaction between **BCN-C10** and compounds **3**, **4** and **7** were carried out in methanol at 25°C under pseudo-first order conditions, with BCN-C10 in at least 10-fold excess. Reactions were followed by monitoring the loss of the substrate absorbance spectrophotometrically at a suitable wavelength (see Figures S8 and to S9 for details). Observed pseudo-first-order rate constants, k_{obs}, were obtained using nonlinear regression of the monoexponential loss of absorbance with time. Second order rate constants, k_2, were obtained from linear regression of plots of k_{obs} against BCN-C10 concentration. Second order plots are shown in Figures S8 and S9.The reactions were carried out at 25˚C using a Pharmacia Ultrospec 2000 UV-visible spectrophotometer.

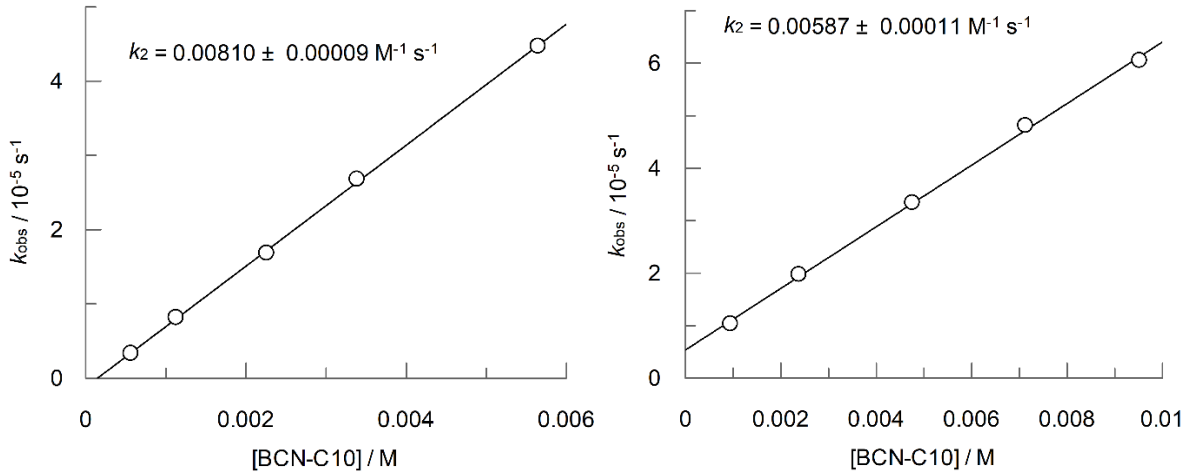

Figure S8: Plot of observed pseudo-first-order rate constant, k_{obs}, against BCN-C10 concentration for the reaction with complexes **3** (left) and **4** (right). The slope, which is equal to the second order rate constant, k_2, is shown on the plot. The reactions were carried out in methanol at 25°C under pseudo-first-order conditions, with $[\mathbf{3}]_0$ = 3.92 x 10^{-5} M, $[\mathbf{4}]_0$ = 4.76 x 10^{-5} M and **BCN-C10** concentrations as detailed on the x-axis. Pseudo-first-order rate constants, k_{obs}, were obtained from measuring the monoexponential decay in absorbance at 412 nm using non-linear least squares analysis.

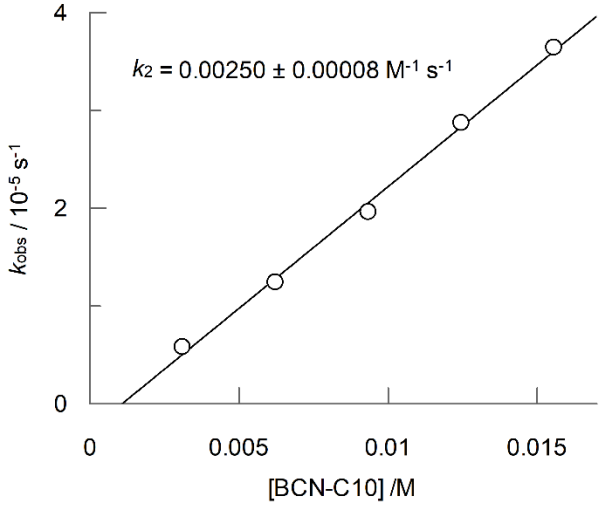

Figure S9: Plot of observed pseudo-first-order rate constant, k_{obs}, against **BCN-C10** concentration for the reaction with ligand **7**. The slope, which is equal to the second order rate constant, k2, is shown on the plot. The reactions were carried out in methanol at 25°C under pseudo-first-order conditions, with $[\mathbf{7}]_0 = 3.92 \times 10^{-5}$ M and BCN-C10 concentrations as detailed on the x-axis. Pseudo-first-order rate constants, k_{obs}, were obtained from measuring the monoexponential decay in absorbance at 257nm using non-linear least squares analysis.

Computational analysis

Calculation details

Calculated transition states were determined for reactions of compounds **6**, **7**, **2** and **3** with BCN. Experimental rate constants were obtained using slightly different BCN derivatives for **6**/**2** and **7**/**3**, respectively, so for the calculations the OMe BCN derivative shown in Figure S10 was used as a model compound to provide consistency across the calculations. All DFT calculations were performed using Gaussian 16.[5] Calculations were carried out using the M06 functional[6] with the 6-311G(d,p) basis set for all first-row elements and the Lanl2dz basis set[7] (with associated pseudopotential) for Ir, along with an additional f polarisation function.[8] Transition states were verified by the presence of a single negative frequency corresponding to motion of the BCN triple bond to/from the carbon atoms of the triazine ring. Gibbs energies were determined at 298.15 K using a quasi-harmonic correction for the entropy term.[9] The IEFPCM solvation model was used to determine solvation energies in methanol. For each reaction, multiple feasible transition states exist, so the activation energies given in the main text were derived from the individual activation energies.[10]

Distortion energies were determined as the difference between the energies of the reactant geometries taken from the transition states and their respective optimised energies. Interaction energies were determined as the difference between the sum of isolated reactants (in the transition state geometries) and the optimised transition states. Overlap integrals were calculated using Multiwfn.[11]

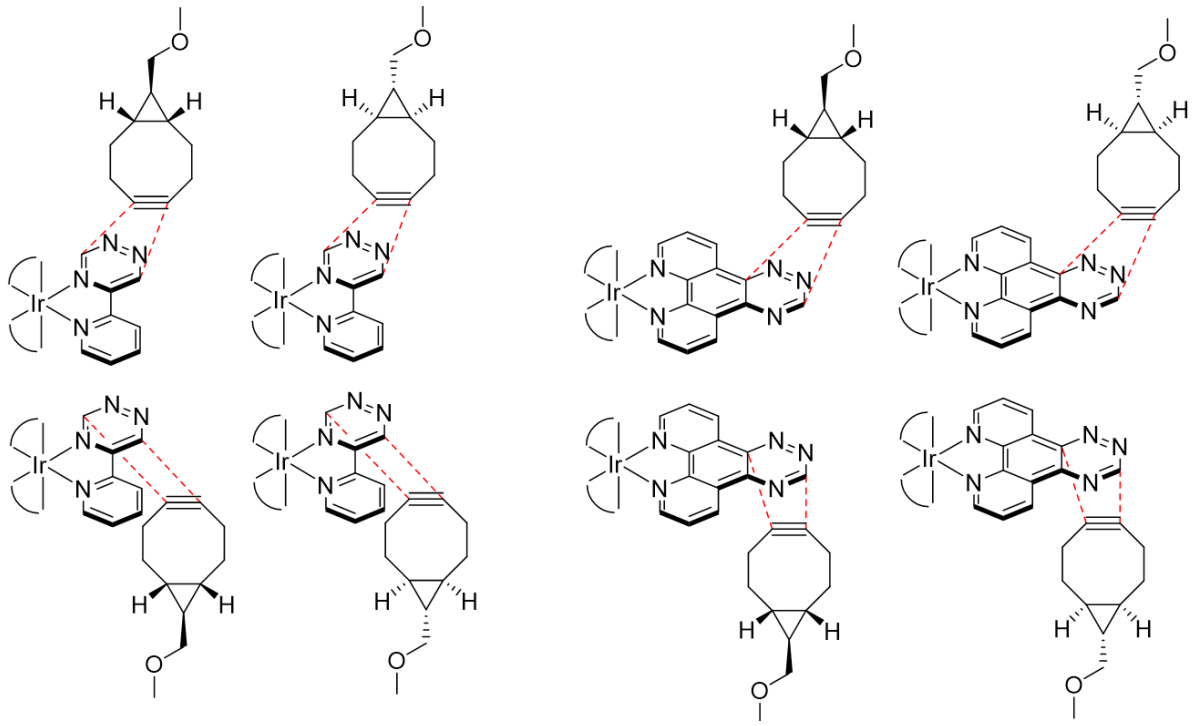

Figure S10. Schematic illustration of the transition states calculated for compounds **2** and **3** (left and right, respectively). Equivalent transition states were calculated for compounds **6** and **7**, but due to the symmetry of the triazines only two transition states were required.

Table S1. Calculated distortion and reaction energies for the lowest energy transition states of the reactions.

Compound	E_{dist} (diene) / kJ mol^{-1}	E_{dist} (dienophile) / kJ mol^{-1}	E_{dist} (sum) / kJ mol^{-1}	E_{int} / kJ mol^{-1}
6	69.0	11.4	80.4	–38.3
2	67.7	10.6	78.3	–103.2
7	80.5	16.9	97.5	–48.5
3	77.4	16.2	93.6	–72.5

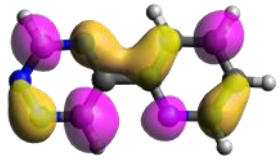

6 (LUMO+1)

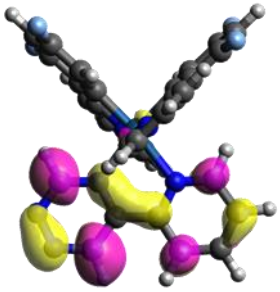

2 (LUMO+1)

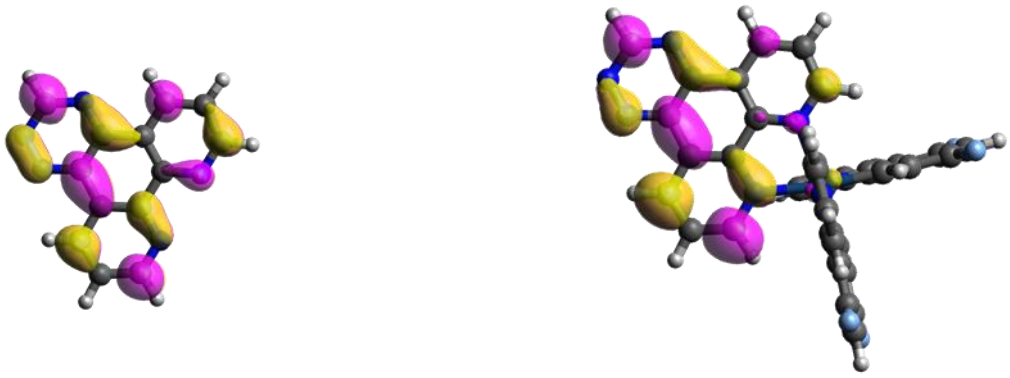

7 (LUMO+1) **3** (LUMO+2)

Figure S11. Visualisations of the frontier orbitals of the dienes with an iso level of 0.03. All compounds are oriented with the same triazine orientation.

Table S2. Calculated frontier orbital energies, energy gaps, and calculated frontier orbital overlap integrals for the lowest-energy transition state geometries.

Compound	Diene frontier orbital energy / eV	BCN HOMO energy / eV	Frontier orbital energy gap / eV	Overlap integral
6	–2.27	–6.88	4.61	0.113
2	–6.03	–6.87	0.84	0.082
7	–2.68	–6.87	4.19	0.118
3	–5.72	–6.85	1.14	0.116

Photophysical properties

Absorption spectra were recorded on a Cary 300 UV−visible spectrophotometer (Varian) and emission spectra at room temperature were carried out with a FLS-1000 from Edinburgh Instruments equipped with photomultiplier (PMT) and those in rigid matrix at 77 K were recorded on a Horiba Fluoromax 4. Quartz cuvettes with 1 cm optical path were used. Lifetimes were measured using LP900 spectrometer with a Flashlamp pumped by Q-switched Nd:Yag laser operating at 355 nm (77 K) and with a PMT detector, or with a picosecond laser diode operating at 410 nm and using a time-correlated single photon counting detection (TCSPC, PicoHarp 300). Emission quantum yields in solution were determined in deaerated solutions at room temperature, and calculated with the following equation.

$$QY_s = QY_{ref} \times \frac{I_s}{I_{ref}} \times \frac{A_{ref}}{A_s} \times \left(\frac{\eta_s}{\eta_{ref}}\right)^2$$

$\mathbf{QY_s}$ corresponds to the quantum yield of the sample to be analysed, $\mathbf{QY_{ref}}$ is the quantum yield of the reference compound, **I** corresponds to the intensity of the emission (area of the spectrum), **A** is the absorption at the excitation wavelength, **η** corresponds to the refractive index of the solvents.

The two properties that provide information about the excited state beside the shape of the emission are the **QY** (Φ) and lifetime (τ), represented the following equations.

$$\Phi = \frac{k_r}{k_r + k_{nr}} \quad \tau = \frac{1}{k_r + k_{nr}}$$

The radiative (k_r) and non radiative (k_r) constants can obtained from combination and rearrangement of the **QY** (Φ) and τ equations to give equations:

$$k_r = \frac{\Phi}{\tau} \qquad k_{nr} = \frac{1}{\tau} - k_r$$

Singlet oxygen generation quantum yield: corrected near infra-red spectra were recorded using a pelletier cooled detector (-20°C), solid indium/gallium/arsenic detector (850–1600 nm). Phosphorescence quantum yields ϕ_Δ were measured in diluted $CHCl_3$ solution with an optical density ≤ 0.1 using the Stern–Volmer plot method based on following equation:

$Qx/Qr = [A_r/A_x\,][\eta_x\,2/\eta_r\,2][Dx\,/Dr\,]$

$$\Phi\Delta_x = \Phi\Delta_r \, X \, \frac{I_x}{I_r} X \frac{A_r}{A_x} X \left(\frac{\eta_x}{\eta_r}\right)^2$$

where A is the absorbance at the excitation wavelength, η the refractive index and D the integrated luminescence intensity. "r" and "x" stand for reference and sample respectively. Here, the reference was perinaphthenone (ϕ_Δ = 0.98 in $CHCl_3$)**.** Excitation of reference and sample compounds was performed at the same wavelength.

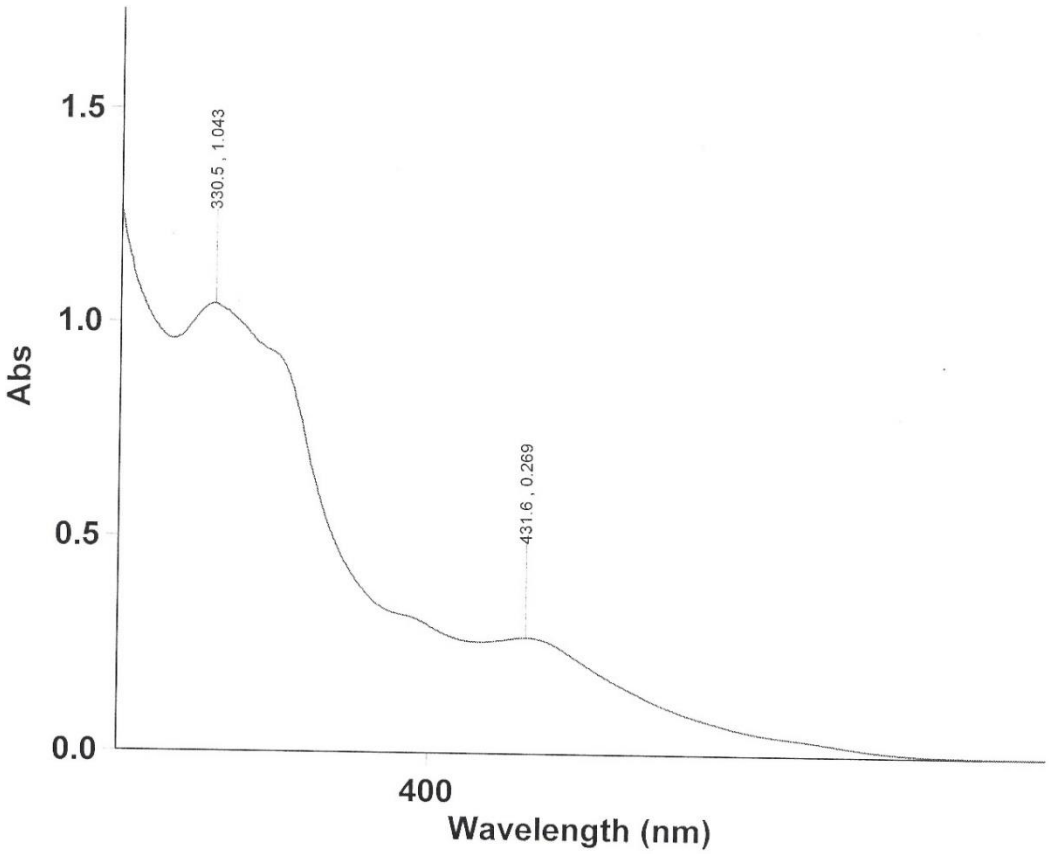

Figure S12. Absorption spectrum of **4** in ethanol ($4.03*10^{-5}$M)

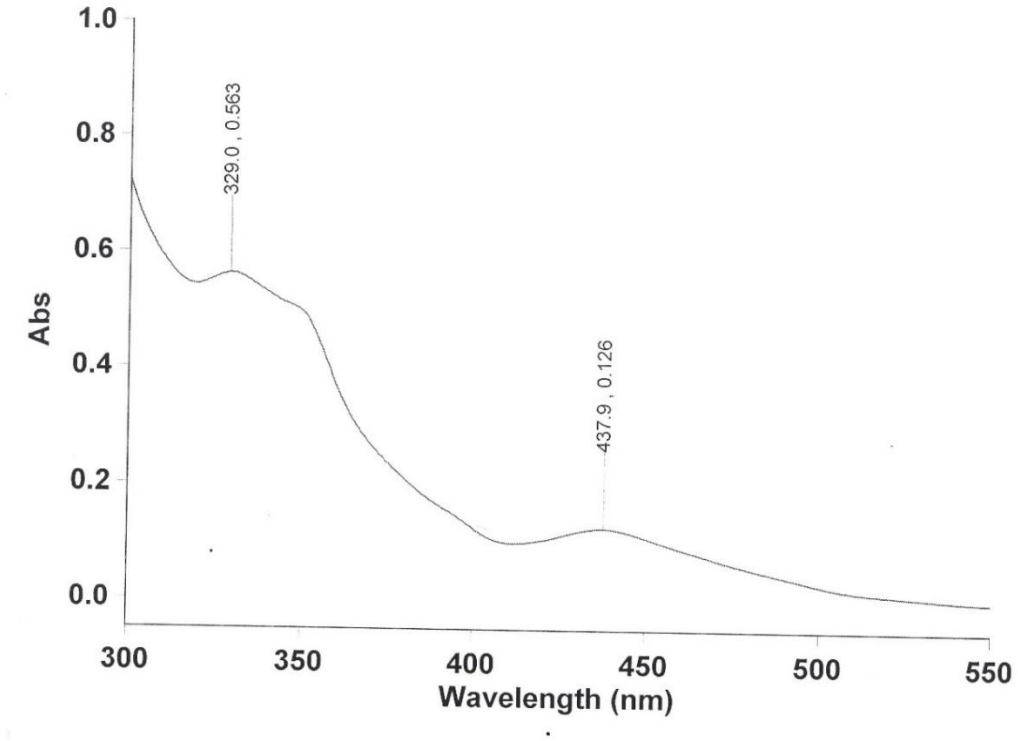

Figure S13. Absorption spectrum of **8** in ethanol ($2.47*10^{-5}$M)

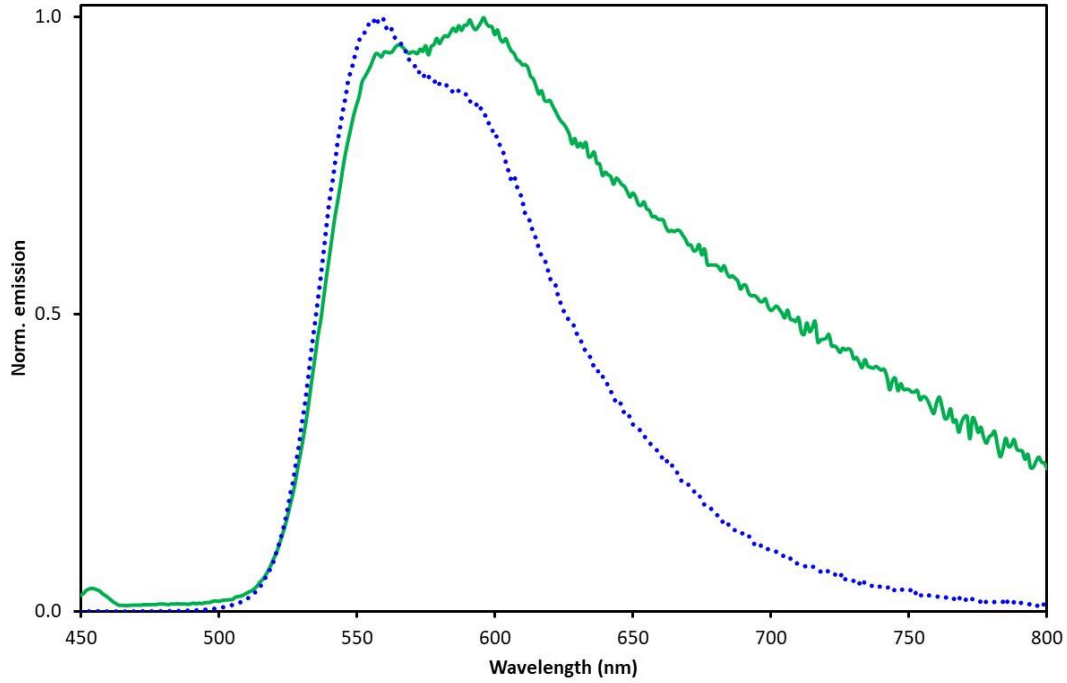

Figure S14. Emission spectra of complex **4** (full line) and complex **8** (dash line) in CH_2Cl_2 at r.t.

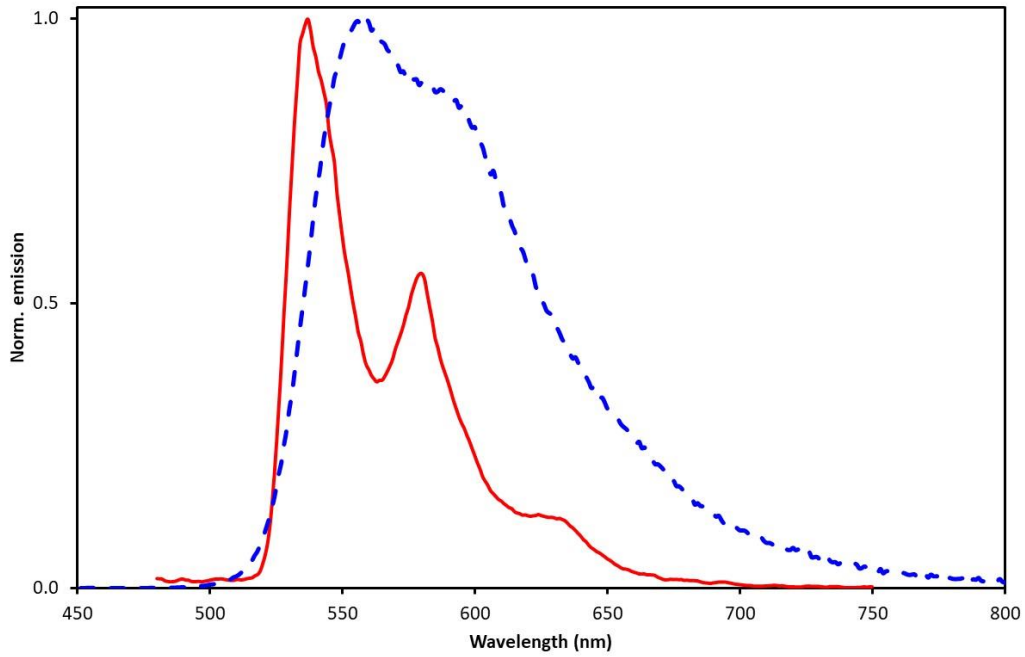

Figure S15. Emission spectra of complex **8** in benzonitrile at 77 k (red) and in CH_2Cl_2 at r.t. (dash blue line).

Uptake of complex **8** by Jurkat cells determined by flow cytometry

Method

Jurkat cells (ATCC® TIB-152™) were maintained in complete RPMI (RPMI (Sigma Aldrich) with 10% FCS, 5% penicillin/streptomycin and 5% L-Glutamine) at 37^{0}C, 5% CO_2. Cells were counted, washed and maintained in sterile PBS (Sigma Aldrich) at 5x10^6/ml for staining experiments in round bottom polystyrene FACS tubes (Corning™ Falcon™). 2.5x10^6 cells were incubated per tube with complex **8** at 1µM (stained) or PBS (control) at 37^{O}C, 5% CO_2 for 30 minutes. Cells were then washed in PBS x3 by centrifugation at 400xg and resuspended in PBS for analysis using a FACSCanto II flow cytometer (Becton, Dickinson and Co., Franklin Lakes, NJ, USA) with an excitation wavelength of 488 nm. The number of events analysed per sample was set at 10,000 .

Results

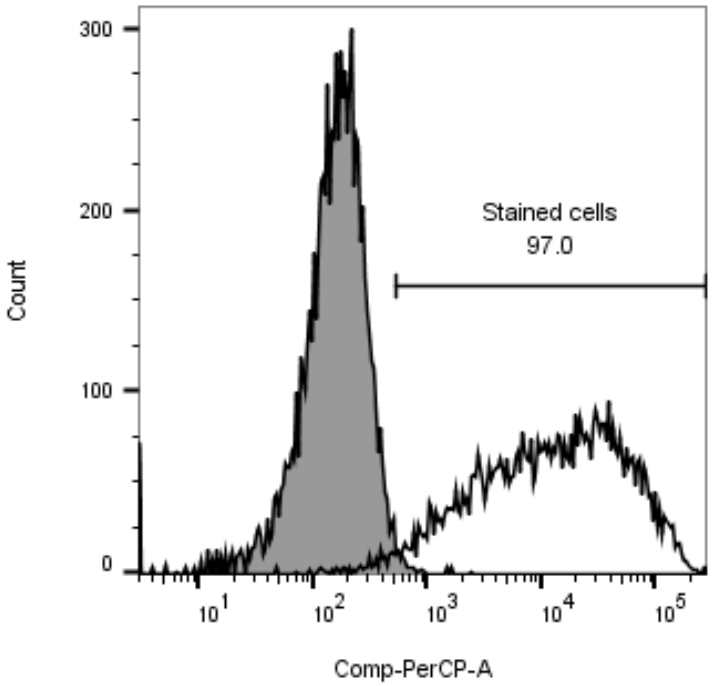

Figure S16. Complex **8** staining of Jurkat cell line. 97% of cells within the stained sample (clear) demonstrated increased fluorescent compared to the negative control sample (grey) as visualised by flow cytometry

Comparison of stained cells and negative controls demonstrated that 97% of the cells treated with complex **8** emitted detectable fluorescence. This demonstrates that complex **8** is capable of staining mammalian cells in culture.

Uptake and localisation of complex **8** in HeLa cells

General

HeLa cells were maintained in DMEM media (Invitrogen) supplemented with 10% fetal bovine serum (FBS) and maintained in a 5% CO_2 humidified 37°C incubator. HeLa cells were grown on glass coverslips at 1 x 10^5/ml overnight at 37°C in 6 well plates. HeLa cells were washed in 1x phosphate buffered saline (PBS) and then incubated with complex **8** (10mM) in Optimem media (Invitrogen) media for 30 mins at 37°C, 5% CO_2 humidified atmosphere. Following incubation, cells were washed with 1xPBS, then fixed with 2% paraformaldehyde in PBS for 10 mins at room temperature followed by washing with 1x PBS. Coverslips were mounted using 4',6-diamidino-2-phenylindole (DAPI) mounting media (Gibco) onto microscope slides. For counterstaining, HeLa cells were incubated with Mitospy RED (0.25mM, BioLegend) in Optimem media for 30 mins at 37°C, followed by washing with 1x PBS and counterstaining with complex **8** (1.25mM) as previously described. Counter-stained HeLa cells were mounted using Hydromount.

Images were acquired on a Leica DMi8 inverted SPE laser scanning confocal microscope using a Leica apochromat 63x/1.30 oil immersion objective. Pinhole size was set to 1 AU. 512 x 512 pixel images were acquired using PMTs detectors. The following settings for each channel were used to acquire images within the respective channels; DAPI, 405nm excitation at 89.6μW, emission 430-480nm, 1.44 μs (dwell time) 800 (gain) and 0 (offset). Complex **8** 488nm excitation at 106.7μW, emission 500-650nm, 1.44 μs (dwell time) 800 (gain) and 0 (offset). MitoSpy red, 561nm excitation at 139.2μW, emission 570-700nm, 1.44 μs (dwell time) 800 (gain) and 0 (offset). Analysis of individual and counterstained images were performed using *imageJ* software.

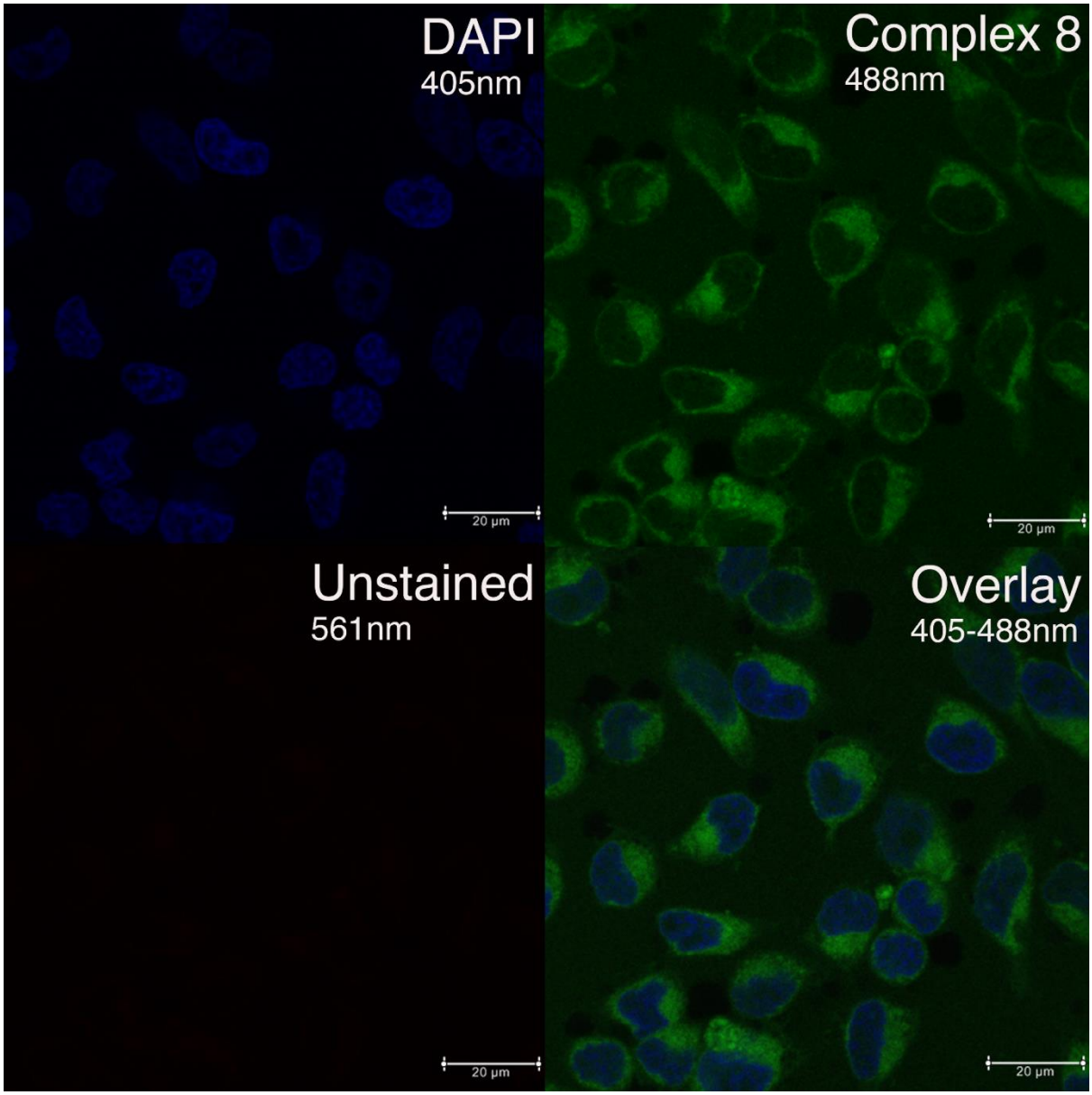

Figure S17. Confocal images of HeLa cells. HeLa cells were stained with complex **8** (10mM), counterstained with the nuclear DAPI dye and analysed by confocal microscopy. The DAPI 405nm channel demonstrates nuclear staining (blue). Complex **8** 488nm channel demonstrates cellular staining of **8** (green). No apparent complex **8** fluorescence can be detected in the MitoSpy red 561nm channel. Overlay demonstrates distinct complex **8** (green) and nuclear (DAPI, blue) localisation.

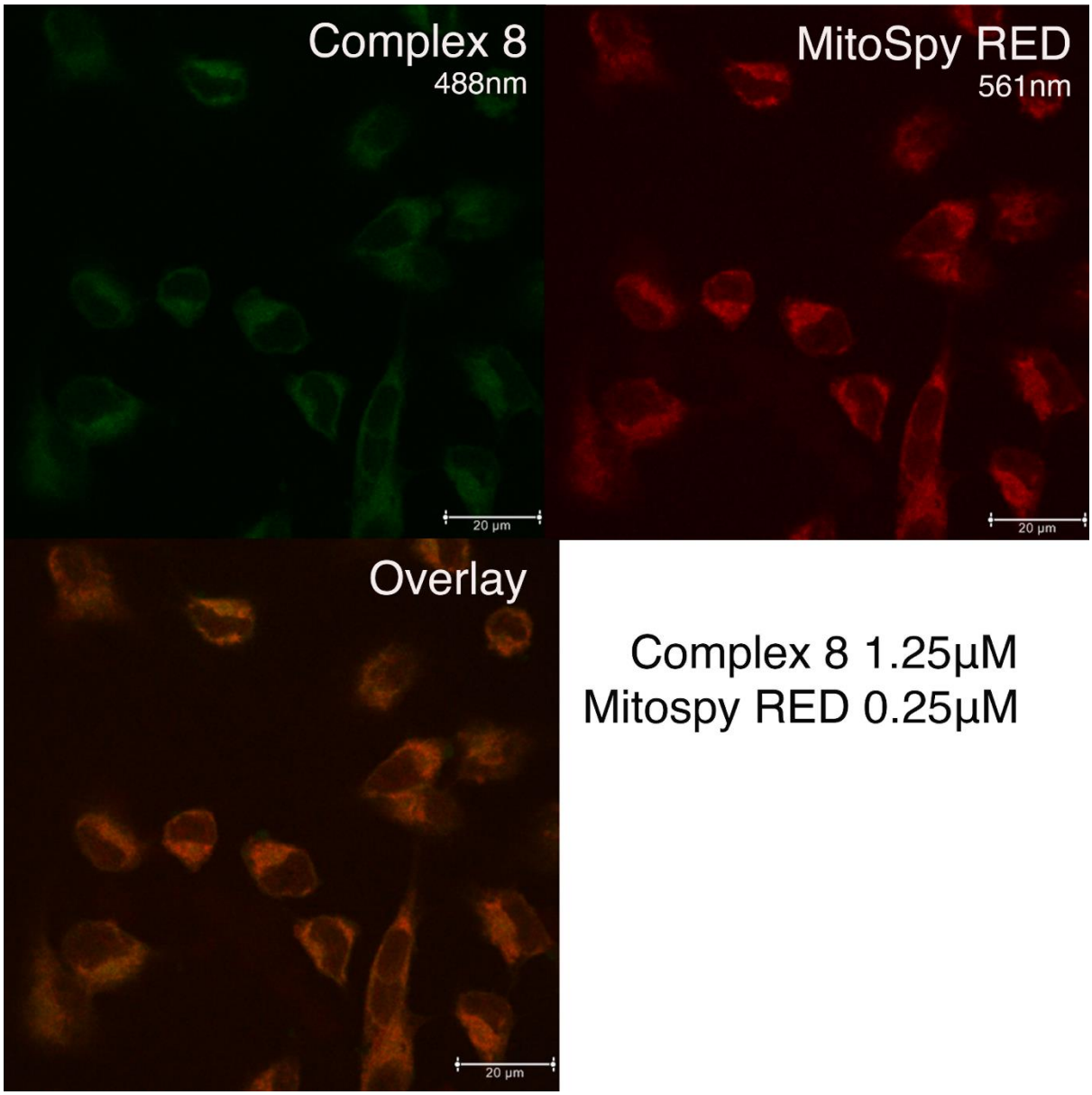

Figure S18. HeLa cells co-stained with MitoSpy red and complex **8**. HeLa cells were stained with mitospy RED (0.25mM, 561nm, upper right panel) and counterstained with 8 (1.25mM, 488nm, upper left panel) followed by confocal microscopy analysis. Overlay demonstrates a degree of co-distribution between **8** and MitoSpy red (lower left panel).

“Chemistry on the complex” to prepare luminescent antibody conjugates.

General Methods

All materials were obtained from Fisher Scientific unless otherwise specified and used without any further purification. Deionised water was obtained using a Select Fusion ultrapure water deionisation system (Suez) with a resistance of >18.2 MΩ/cm at 25 °C. Absorbance measurements were obtained using a NanoDrop One$_c$ Microvolume UV-Vis Spectrophotometer (NanoDrop Technologies, Inc.).

Spectral Analysis

Absorption spectra for each fluorescent iridium complex (100 µM) were acquired on a NanoDrop One at 0.5 nm intervals between 190 – 850 nm. Emission spectra for each fluorescent iridium complex (10 µM) were acquired on a RF-6000 Spectrofluorophotometer (Shimadzu) at 0.5 nm intervals between 450-900 nm. The absorption and emission maxima for each complex were subsequently determined within 0.5nm from these spectra.

Synthesis of amine-reactive complexes 9 and 10.

Aliquots of the triazine iridium(III) complexes (**3** and **4)** were combined with aliquots of amine-reactive **BCN-PNP** to achieve a 10% molar excess, in DMSO or DMSO-d_6. The final reaction mixture (300 – 500 µL) was incubated at 50°C overnight (16 hours) at 450 rpm. Sample of the complex **3** reaction mixture following incubation was analysed by ^{1}H NMR to confirm the reaction had run to completion, through the absence of any remaining amine-reactive **BCN-PNP**. The concentration of the click product was calculated based on the product yield determined by NMR.

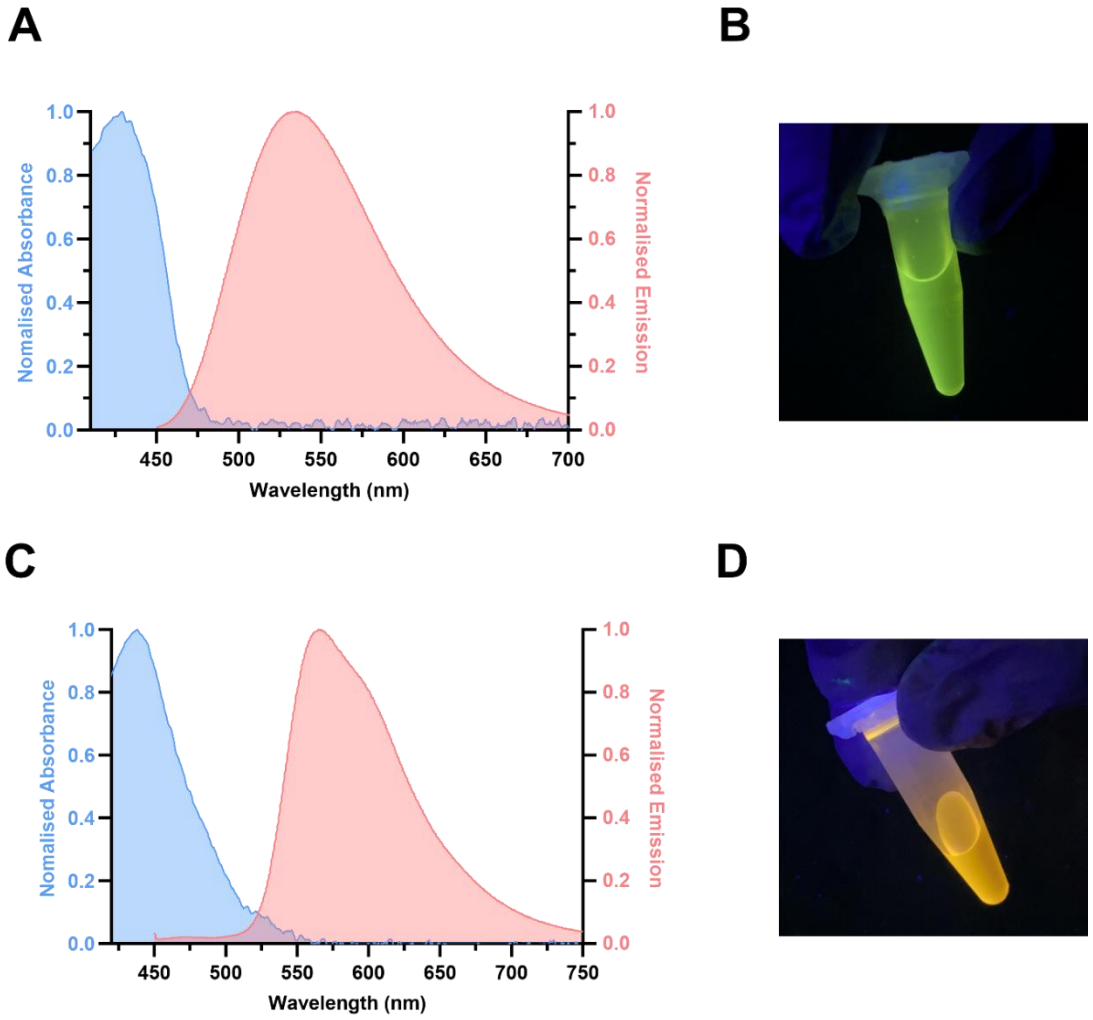

Figure S19. Spectrophotometric analysis of the amine-reactive-iridium click products. Normalised absorption (blue, 100 µM, in DMSO) and emission (red, 10 µM, in DMSO) spectra of amine-reactive complex **9** (A) and amine-reactive complex **10** (C). Iridium complexes fluoresce under a UV lamp (λex. 365 nm), B) amine-reactive complex **9**, D) amine-reactive complex **10**.

Bioconjugation

Aliquots of 1.5 mg of lyophilised trastuzumab were dissolved in 500 µL of 0.1 M $NaHCO_3$ (pH 8.3) and washed three times in pre-rinsed 30 kDa MWCO 0.5 mL centrifugal filters (Amicon) at 12,000 × g for 8 minutes. Following each spin cycle, 0.1 M $NaHCO_3$ (pH 8.3) was added to maintain a total volume of 500 µL. The purified antibody was collected from the filters at 2,500 × g for 3 minutes and the concentration adjusted to 5 mg/mL with buffer based on absorbance measurements. The antibody and dye solutions were both heated to 37°C prior to their combination to aid with solubility. Once heated, a 30-fold molar excess of the amine-reactive complex **9** or **10** stock solution in DMSO-D_6 or DMSO was slowly added to the antibody solution (500 µg, 200 µL final volume, DMSO % v/v = 10 %) with constant stirring and incubated at 37 °C for 1 h at 500 rpm.

Bioconjugate Purification

Following bioconjugation, 300 µL of PBS (pH 7.4, preheated to 37 °C) was added to the crude trastuzumab conjugate **11** or **12** and washed at 37 °C in pre-rinsed 30 kDa MWCO 0.5 mL centrifugal filters, as per the speed and durations detailed in the above section. The bioconjugate solution was retrieved from the filter, along with small amounts of precipitate and the supernatant was removed for further purification. The conjugates **11** and **12** were then purified through Zeba™ Dye and Biotin Removal Spin Columns, as per the supplier's instructions. Each bioconjugate solution was passed through two columns, as recommended in the instructions for molar excesses of dye greater than 10-fold.

Degree of Labelling Determination

The mean number of iridium complexes conjugated to each antibody (DOL_{Ir}) in the purified immunoconjugate solution was calculated using the following equations:

$$DOL_{8PF6} = \frac{A_{402} \times MW\ [Ab]}{Ab\ conc.\left(\frac{mg}{mL}\right) \times\ \varepsilon\ [Ir\ complex]}$$

where:

$$Antibody\ Concentration\ (mg/mL) = 10 \times \frac{A_{280} - (A_{402} \times CF)}{\varepsilon_1\%\ [Ab]}$$

CF = correction factor (A_{280}/A_{430}), $\varepsilon_1\%$ = percent molar attenuation coefficient for a 10 mg/mL IgG solution.

The molar attenuation coefficients (ε) and correction factors of complex **9** (ε = 6,800 $M^{-1}\,cm^{-1}$; CF = 11.59) and complex **10** (ε = 8,363 $M^{-1}\,cm^{-1}$; CF = 10.61) were determined from standard curves via UV-vis absorption spectrophotometry.

SDS-PAGE

Trastuzumab-iridium conjugates **11** and **12** were analysed by sodium dodecyl sulphate-polyacrylamide gel electrophoresis (SDS-PAGE). Antibody samples (≤ 6.5 µL, concentration dependent) were prepared by adding 2.5 µL sample buffer (NuPAGE™ 4X LDS sample buffer, Invitrogen) and deionised water (≤ 6.5 µL, concentration dependent), to a total volume of 10 µL. The samples were protected from light by aluminium foil and incubated at 70 °C for 10 minutes at 450 rpm. Protein molecular weight standards (ThermoScientific PageRuler Unstained Broad Range Protein Ladder) and antibody samples were loaded into a 10-well mini protein gel (NuPAGE™ 3-8% Tris Acetate, 1.0 – 1.5 mm, Invitrogen) and ran for 1 h at 135 V in NuPAGE™ 1X Tris-Acetate SDS Running Buffer, Invitrogen. The gel was washed three times in 200 mL deionised water for 5 min prior to staining with 50 mL 1X SYPRO® Red Protein Gel Stain for 1 h. Following staining, the gel was briefly destained by washing for ≤ 1 min in 1

M acetic acid, then washed once more in deionised water prior to imaging. The gel was scanned using an ChemiDoc MP (BIORAD) for SYPRO® Red (λex. = 625 – 650 nm [Epi-red], λem. = 675 – 725 nm) and iridium complexes (λex. = 302 nm [UV-trans], λem. = 535 – 645 nm).

Cytotoxicity and bioorthogonal reactivity of the complexes.

General

3-(4,5-dimethylthiazol-2-yl)-2,5-diphenyltetrazolium bromide (MTT) and cell culture relevant reagents such Dulbecco's modified Eagle's medium (DMEM), fetal bovine serum (FBS), antibiotics (penicillin, streptomycin), phosphate buffered saline (PBS), trypsin were all purchased from Sigma-Aldrich Chemical Co., St. Louis, MO, USA.

Cell lines and culture conditions

A-375 (human melanoma) cell lines were obtained from the American Type Culture Collection (ATCC, Manassas, VA, USA) and HFF-1 cells were a gift from PAVAL Lab from Grenoble Alpes University. A-375 and HFF-1 were grown in DMEM supplemented with 10% FBS, 1% penicillin and streptomycin at 37°C under 5% CO2 atmosphere.

Cell viability assay

Cytotoxicity of the Iridium triazine complexes **3** and **4** were measured using MTT (3-(4,5-Dimethylthiazol-2-yl)-2,5-diphenyltetrazolium bromide) assay as previously described. [12] Cells were seeded into 96-well plates ($4x10^3$ cells.well^{-1} for A-375 and $1.8x10^3$ cells x well^{-1} for HFF-1) in 200 µL of culture medium and allowed to attach for overnight. Cells were then treated with each complexes in a range concentration of 0.78 to 100 µM for 24h, 48h and 72h. MTT solution (0.5 mg x mL^{-1} in culture media) was added to each well and the cells were further incubated at 37°C for 4h. Subsequently, the media was removed, and the blue formazan crystals were dissolved in 100 µL of DMSO. The absorbance value was read at 570 nm on a POLARstar Omega plate reader (BMG labtech) and the cell viability was calculated using the following formula:

$$Cell\ viability\ (\%) = \left(\frac{OD_{Sample} - OD_{Blank}}{OD_{Control} - OD_{Blank}}\right) \times 100$$

Confocal microscopy

Cells were seeded onto coverslips in 8-wells labtek with a cell density of $2x10^4$ cells per well and allowed to attach for 24h. Ac_4man*N*BCN was then added directly to the medium in wells (50 µM final concentration) and the culture was continued for 48h. The culture medium was then removed and cells were washed two times with PBS prior to be incubated with 10 µM complex **4** (diluted in the medium) for 30 min at 37°C. Control cells not-pre-incubated with BCN-sugar received the same treatment. Cells were then imaged with confocal microscope using a TCS SP8 GSU Leica (HC PL APO CS2, 40X/1.30 OIL, zoom 3.2, with an image resolution of 1024 x 1024 pixels). Excitation wavelength was 488 nm and emission was collected in the 520 - 620 nm range. Images were processed using ImageJ software. [13]

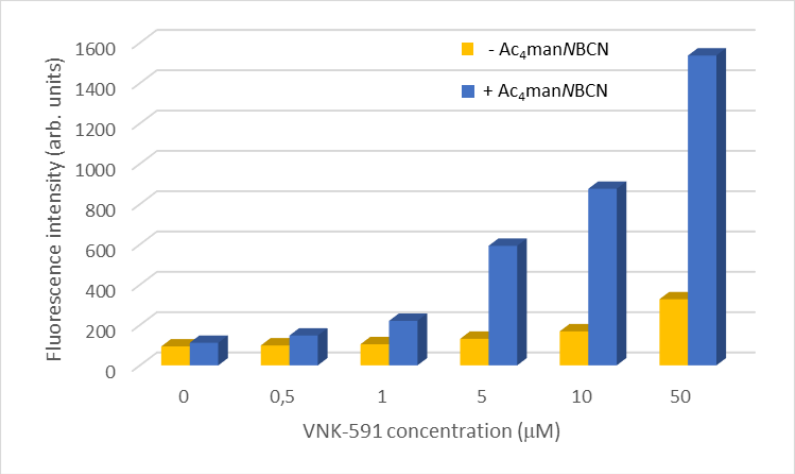

Figure S20. Effect of increasing concentration of complex **4** on the fluorescence of A-375 cells pre-incubated or not with Ac$_4$man*N*BCN.

Flow cytometry

A-375 cells were seeded at a density of 15x10^4 cells in 6-well plates and were allowed to attach for 24h. Ac$_4$man*N*BCN was then added directly to the medium in wells (50 µM final concentration) and the culture was continued for 48h. The culture medium was then removed and cells were washed two times with PBS prior to be incubated with various concentrations of complex **4** (diluted in the medium) for 30 min at 37°C. Control cells not-pre-incubated with BCN-sugar received the same treatment. Cells were then washed again once with PBS then were detached by treatment with 0.5 mL/well of trypsin-EDTA for 5 min at 37°C. Afterwards, the harvested cells were centrifuged, washed with 1 mL of PBS and resuspended in 500 µL of PBS for analysis by flow cytometry. Flow cytometry analysis was performed on a BD LSR FORTESSA Flow cytometer (laser excitation at λ=488 nm, emission bypass filter at 575/26).

Stability studies.

A.

t= 0 min

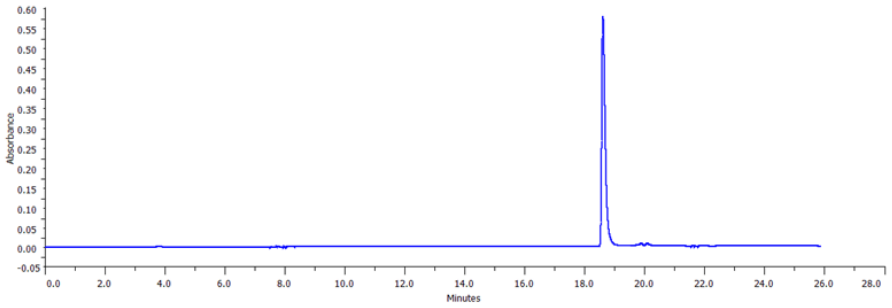

t= 4h

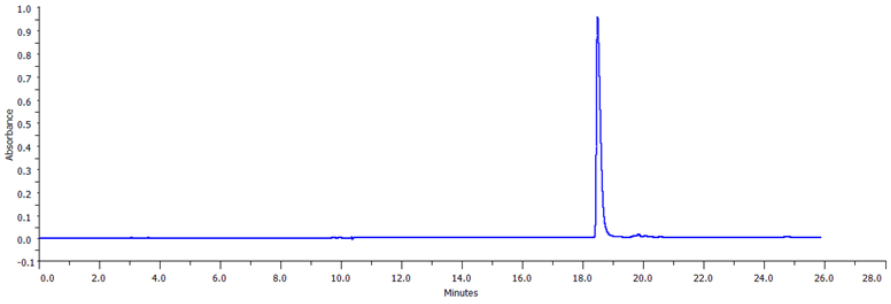

t= 24h

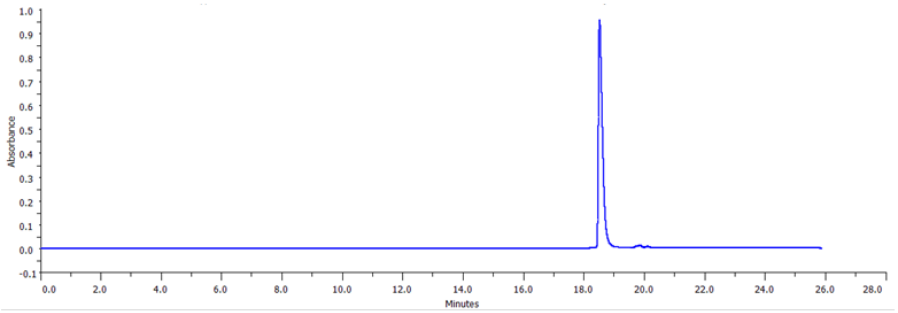

t= 48h

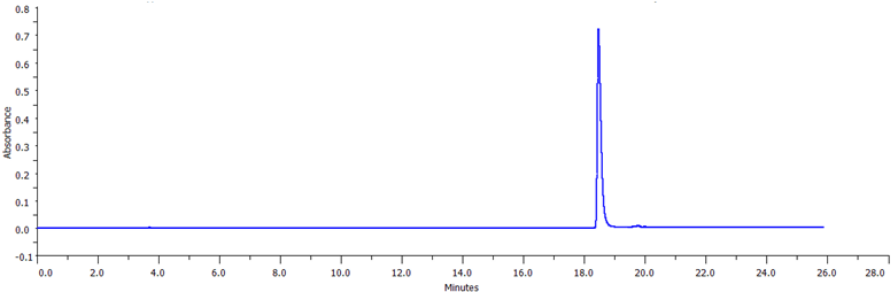

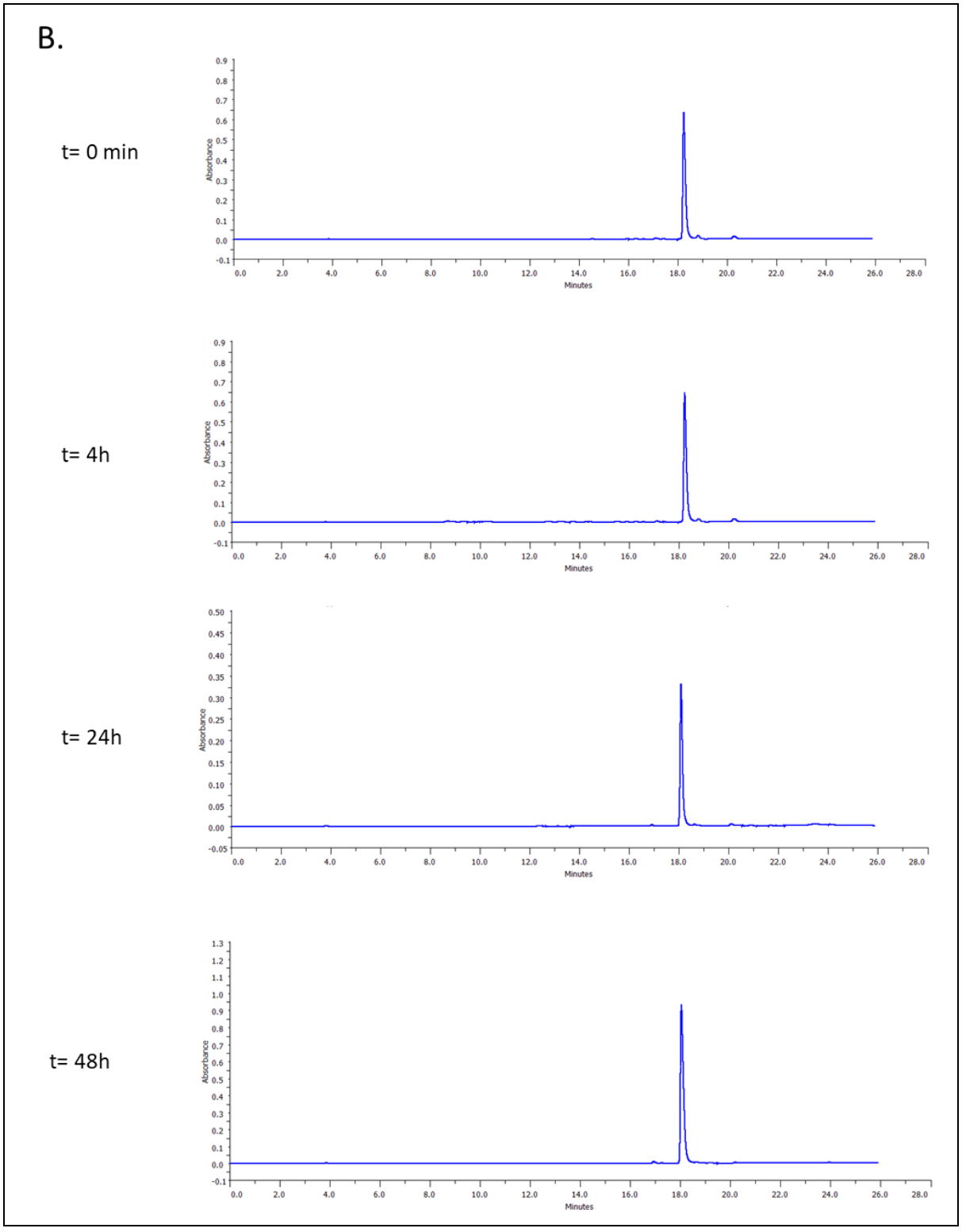

Figure S21. HPLC profile (260 nm) of the iridium complexes **4** (A.) and **3** (B.) incubated in PBS, pH 7.4 at 37°C for t=0 – 4 – 24 and 48 hours. A VP250/4.6 Nucleosil 100-7 C18 column (Machery-Nagel) was used with a linear gradient of Acetonitrile:water 90/10 (v/v) in 50 mM

triethylammonium acetate, pH 7.0 in 10% (v/v) acetonitrile (20 to 100% during 20 min) at a flow rate of 1 mL/min.

References

1. W. Li, H. Pan, H. He, X. Meng, Q. Ren, P. Gong, X. Jiang, Z. Liang, L. Liu, M. Zheng, X. Shao, Y. Ma and L. Cai, *Small*, 2019, **15**, 1804383.

2. L. C.-C. Lee, J. C.-W. Lau, H.-W. Liu and K. K.-W. Lo, *Angewandte Chemie International Edition*, 2016, **55**, 1046-1049.

3. G. R. Pabst, O. C. Pfu¨ller and J. r. Sauer, *Tetrahedron Letters*, 1998, **39**, 8825-8828.

4. H. Neunhoeffer and F. Weischedel, *Justus Liebigs Annalen der Chemie*, 1971, **749**, 16-23.

5. M. J. Frisch, G. W. Trucks, H. B. Schlegel, G. E. Scuseria, M. A. Robb, J. R. Cheeseman, G. Scalmani, V. Barone, B. Mennucci, G. A. Petersson, H. Nakatsuji, M. Caricato, X. Li, H. P. Hratchian, A. F. Izmaylov, J. Bloino, G. Zheng, J. L. Sonnenberg, M. Hada, M. Ehara, K. Toyota, R. Fukuda, J. Hasegawa, M. Ishida, T. Nakajima, Y. Honda, O. Kitao, H. Nakai, T. Vreven, J. J. A. Montgomery, J. E. Peralta, F. Ogliaro, M. Bearpark, J. J. Heyd, E. Brothers, K. N. Kudin, V. N. Staroverov, R. Kobayashi, J. Normand, K. Raghavachari, A. Rendell, J. C. Burant, S. S. Iyengar, J. Tomasi, M. Cossi, N. Rega, J. M. Millam, M. Klene, J. E. Knox, J. B. Cross, V. Bakken, C. Adamo, J. Jaramillo, R. Gomperts, R. E. Stratmann, O. Yazyev, A. J. Austin, R. Cammi, C. Pomelli, J. W. Ochterski, R. L. Martin, K. Morokuma, V. G. Zakrzewski, G. A. Voth, P. Salvador, J. J. Dannenberg, S. Dapprich, A. D. Daniels, Ö. Farkas, J. B. Foresman, J. V. Ortiz, J. Cioslowski and D. J. Fox, 2019.

6 Y. Zhao and D. G. Truhlar, *Theor. Chem. Acc.*, 2008, 120, 215–241.

7 P. Jeffrey Hay and Willard R. Wadt, *J. Chem. Phys*., 1985, 82, 270–283.

8 A. W. Ehlers, M. Böhme, S. Dapprich, A. Gobbi, A. Höllwarth, V. Jonas, K. F. Köhler, R. Stegmann, A. Veldkamp and G. Frenking, *Chemical Physics Letters*, 1993, **208**, 111–114.

9 I. Funes-Ardois and R. Paton, GoodVibes: GoodVibes v1.0.1.

10 F. Giralt and R. W. Missen, *The Canadian Journal of Chemical Engineering*, 1974, **52**, 781–783.

11 T. Lu and F. Chen, *Journal of Computational Chemistry*, 2012, **33**, 580–592.

12. T. Mosmann, *Journal of Immunological Methods*, 1983, **65**, 55-63.

13. M. Abramoff, P. Magalhães and S. J. Ram, *Biophotonics International*, 2004, **11**, 36-42.